Validation of a hydrodynamic model for a curved, multi-paddle wave tank

Applied Ocean Research 44 (2014) 39–52

Contents lists available at ScienceDirect

Applied Ocean Research

journal homepage: www.elsevier.com/locate/apor

Validation of a hydrodynamic model for a curved, multi-paddle wave tank

Istvan Gyongy[a,*], Jean-Baptiste Richon[a], Tom Bruce[a], Ian Bryden[b]

[a] Institute for Energy Systems, School of Engineering and Electronics, University of Edinburgh, Edinburgh EH9 3JL, UK
[b] Research & Enterprise Office, University of the Highlands and Islands, Ness Walk, Inverness IV3 5SQ, UK

ARTICLE INFO

Article history:
Received 28 June 2013
Received in revised form 1 October 2013
Accepted 11 November 2013

Keywords:
Wave tank
Wavemaker
Boundary element method
WAMIT
Experimental validation

ABSTRACT

Obtaining a hydrodynamic model for a wave tank has many benefits, from allowing the useable test zone to be identified, to helping with the tuning of the wavemaker controllers. This paper explores a first-order, boundary element method (BEM) that has been previously proposed for modelling wave tanks, applying the method to a tank with a unique, curved geometry. In a series of experiments, the model is shown to provide a good representation of the wave profile across the tank. Inherent limitations in the method are also identified: in the case when only a single paddle is moved, significant, un-modelled second-order spurious waves are found to emerge. Moreover, the representation of the wave absorbers by a simple, partially reflecting surface does not adequately reproduce the measured spatial variation in the reflection coefficient.

1. Introduction

1.1. The Edinburgh curved tank

The Edinburgh curved wave tank [1], which is shown in Fig. 1, was commissioned in 2003 to allow the physical simulation of multi-directional random wave conditions. It utilises an array of force-feedback wave boards (see, for example, Spinneken et al. [2]) to generate waves in a frequency range of 0.5Hz to 1.6Hz and with a directional spread of approximately 60°.

Fig. 2 shows a plan view of the tank. There are a total of 48 wave-making paddles arranged along an arc of radius 9 m that subtends an angle of 96°, with a work platform above the paddles. The paddles are dry back and have a rolling gusset seal. Facing the wavemaker is a bank of wedge-shaped passive absorbers ("beaches"). A wide and deep glass viewing panel, at 90° to the absorber array, completes the tank. The water depth is 1.2 m, and the hinge depth of the paddles is 0.5 m.

Whilst the curved tank is to date unique in featuring a (near) quarter-circular arc of wavemaker segments, there are fully circular wave tanks in existence, namely the Deep Sea Basin at the National Maritime Research Institute in Tokyo [3], the AMOEBA tank in Osaka [4], and FloWave TT [5], a combined current and wave test basin currently under construction at Edinburgh. Table 1 contrasts the main features of these tanks.

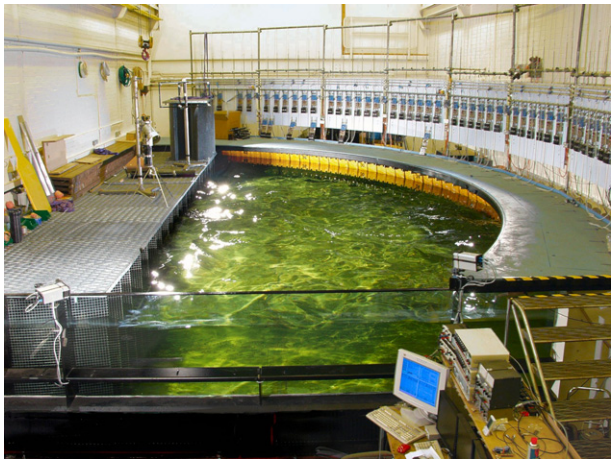

Fig. 1. The Edinburgh curved tank.

Indeed, Naito [6], following a comprehensive review of wave generation and absorption theory, suggests a circular (or elliptical) array of absorbing wave boards as an ideal configuration for a wave tank. The statement is backed up by experimental measurements in the compact AMOEBA tank indicating very similar wave excitation forces to those obtained in much larger wave tanks.

* Corresponding author. Tel.: +44 1316508689.
E-mail addresses: istvan.gyongy@ed.ac.uk (I. Gyongy) j.richon@ed.ac.uk (Jean-Baptiste Richon) tom.bruce@ed.ac.uk (Tom Bruce) ian.bryden@uhi.ac.uk (Ian Bryden).

0141-1187/$ - see front matter © 2013 Elsevier Ltd. All rights reserved.
http://dx.doi.org/10.1016/j.apor.2013.11.002

Table 1
Characteristics of the curved tank and circular tanks.

Tank	Curved tank	FloWave TT	NMRI	AMOEBA
Geometry	Curved	Circular	Circular	Circular
Radius	9 m	12.5 m	7 m	0.8 m
Actuator	48 force-feedback, dry back paddles	168 force-feedback, dry back paddles	128 position-feedback, wet back paddles	50 force-feedback plungers
Depth	1.2 m	2 m	5 m	0.25 m
Maximum wave height	0.12 m	0.7 m (planned)	0.5 m	0.02 m
Frequency range	0.5–1.6 Hz	0.3–1 Hz (planned)	0.25–2 Hz	1.6–3 Hz

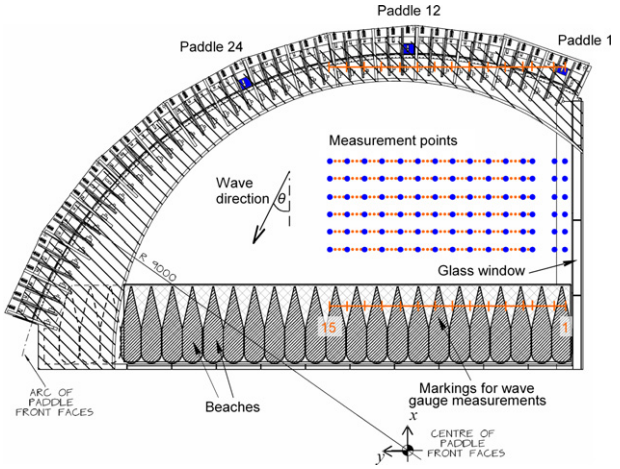

Fig. 2. Plan view of the curved tank.

1.2. The operation of the tank

At the simplest level, the generation of waves in the curved tank can be considered as a generalisation of the "snake" approach which has been used in multidirectional waves for decades and is widely discussed in the literature (for example, Jeffrey et al. [7] and Linfoot et al. [8]). In principle, the wavemaker can be considered as an arc of finite-width sources. Sinusoidal signals are sent to the individual wavemaker segments, through an appropriate control system, with phase and amplitudes adjusted to generate unidirectional waves with preset periods, directions and amplitudes.

An important distinction between using force control rather than position control of the wavemaker, as emphasised by Spinneken et al. [2], is that in force control the generated wave field directly feeds back into the wave generation process. One of the consequences is that the wavemaker "senses" and tends to compensate for some of the spurious free waves at harmonics of the desired wave frequency. Furthermore, by incorporating the wave board velocity into the force feedback loop, effective wave absorption can be obtained, without requiring wave gauges in front of the paddle to measure the incident waves [9].

Once it is assumed that control algorithms are available to generate travelling waves with defined heights, periods and directions, then, in principle, it is possible to combine signals to the wavemaker linearly to create physical simulations of random seas, the frequency and directional statistics of which can be defined according to any available parametric spectra (see, for example, Ochi [10]), such as the Pierson-Moskowitz, JoNSWAP, ITTC or ISSC.

In the curved tank, the required wavemaker demand signals are computed by taking the inverse discrete Fourier Transform of the desired spectrum, and applying a pseudo-random generator to imitate the stochastic nature of the sea [11]. The resulting physically simulated random sea states in the curved tank are repeating complex-periodic processes, which do not require window functions to be applied in the analysis of recorded wave elevations. This has a significant advantage when it comes to measuring wave spectra for validation purposes, as it allows for more accurate spectral estimates [12].

1.3. Modelling 3D wave tanks

Whilst snake theory gives a useful approximation of the wave field generated by a segmented wavemaker, it does not account for the geometry of the tank or the exact characteristics of the wavemaker segments. To obtain accurate predictions of the wave field corresponding to a given wavemaker motion, enabling different tank layouts or wavemaker designs (and control schemes) to be assessed, one has to consider more sophisticated models.

One of the first studies looking at the limitations of snake theory was Sand [13], which investigated the spurious waves that can arise due to the finite width of wave board segments. This was followed by further advances in modelling directional waves in a rectangular tank. Takayama [14] considers each wavemaking segment as a "finite-width" (piston or flap-type) source in an infinitely long wall. The first-order wave field from each wave board (given in closed-form) is then superimposed to obtain the overall wave field, which is found to be in reasonably good agreement with experimental results.

Dalrymple et al. [15] give the first-order solution for finite length and infinitely long wavemakers (both comprised of infinitely narrow segments), as well as point wavemakers. Two scenarios are considered: the wavemaker is either placed in a wall or free standing in the tank. Dalrymple [16] analyses the more practical situation of a closed rectangular tank, with a sloping bottom. A directional wave generation procedure is presented that exploits sidewall reflections to produce uniform planar waves at specified locations within the tank.

An alternative, numerical model is detailed in Isaacson et al. [17] for the wave field in a closed tank with a segmented wavemaker. The method uses linear diffraction theory and a point source representation of the wavemaker and the tank walls, and is experimentally validated in the case of a rectangular tank in Hiraishi et al. [18]. An extension of the technique for partially reflecting boundaries is given in Isaacson [19].

There has also been significant interest in extending wave generation models to second (and higher) order, with a view to derive wavemaker control signals that better reproduce the second-order effects in naturally occurring wave fields, and in particular suppress the generation of second-order spurious waves [20]. Li et al. [21] derive the second-order solution for regular waves generated by a wavemaker at one end of a semi-infinite rectangular basin with reflecting side-walls. A complete second-order wavemaker theory for multidirectional waves (including the second-order control signal) is presented in Schaffer et al. [22], assuming an infinitely long wavemaker. Ducrozet et al. [23] discuss the development and validation of a rectangular, numerical wave tank based on a higher-order spectral method. The numerical tank is seen to provide an accurate prediction

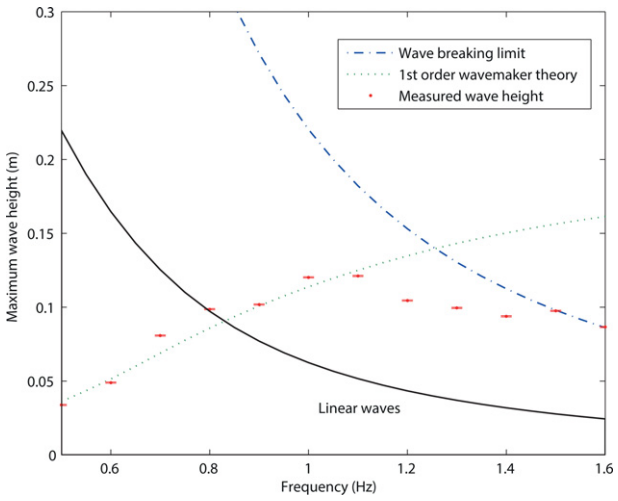

Fig. 3. Limits of regular wave generation in the curved tank.

of irregular wave fields in its real-life counterpart. Fully nonlinear numerical wave tanks, based on finite difference schemes for the Navier–Stokes equations, have also been developed; see for example Park et al. [24].

In practice, second-order, directional wave generation techniques are found to be rather complex to implement, and only limited experimental results have so far been published for these techniques. Whilst Zaman et al. [25] investigate second-order generation in a wave tank, only straight waves are considered. It is also important to note that all the studies on 3D tanks noted above (in effect) assume position-controlled wavemakers (with given motions imposed) rather than absorbing, force-feedback generators. Spinneken et al. [2], in contrast, consider the force control of a rectangular tank, deriving a theoretical first-order transfer function (assuming an infinitely long wavemaker), backed up by experimental observations. In a similar vein, Minoura et al. [26] develop a mathematical formula for generating first-order waves in an arbitrary shaped wave tank, with a segmented, absorbing wavemaker around the perimeter. Polar co-ordinates are adopted and each wavemaker segment is taken to generate a ring wave (expressed using Hankel functions), with evanescent waves being neglected. Reflections from the boundary of the tank are also un-modelled. Experimental results for circular and elliptic configurations of the AMOEBA tank (generating regular, long-crested waves) indicate that the proposed theory gives good wave height predictions for points further than a wavelength away from the wavemaker.

An alternative technique for analysing wave generation and absorption in 3D tanks, which avoids some of the assumptions of analytical approaches, is the boundary element method (BEM). O'Dea et al. [27] and Newman [28] both use commercial BEM solver WAMIT [29] for modelling tanks. The former study investigates the effect of design choices including the type and segmentation of the wavemaker on the quality of waves in a rectangular tank, whilst the latter looks at paddle control strategies in rectangular and circular tanks. However, no experimental data are presented validating the tank models, which are all first-order. The present paper applies the same modelling technique to the Edinburgh curved tank and is believed to be the first study to validate a BEM model for a 3D tank.

1.4. Objectives

In the sections that follow, a first-order hydrodynamic model is presented for the curved tank and the model's wave profile predictions are compared with experimental measurements. Firstly, the capabilities of the tank are outlined in Section 2. Experimental results are given regarding the maximal achievable wave height, together with a summary of the errors in 3D wavemaking and an overview of previous studies on the characteristics of the curved tank. Section 3 describes the boundary element method used to model the tank, and, in particular, the definition of the tank geometry and paddle motion within the model. A method for reproducing the reflection coefficient of the beaches is discussed. The validation experiments are detailed in Section 4. First, descriptions of the experimental setup and procedure are given. This is followed by details on the method of obtaining the required wave height and paddle motion measurements, and an outline of the associated uncertainties. Experimental results are presented next, first for the case when individual paddles are moved at different frequencies, and then for the situation in which all paddles are driven to generate regular, directional waves. In both cases, the wave height profiles predicted by BEM are compared with measurements over a finely spaced grid of points in the tank. Second-order effects, ignored by the model, are discussed, together with possible sources of errors in the BEM estimates. Concluding remarks are given in Section 5.

2. The capabilities of the Edinburgh curved tank

2.1. Wave height and frequency range

The tank is designed to generate small waves in the frequency range 0.5–1.6 Hz. The maximum wave height that can be achieved varies across these frequencies. Taking a regular, monochromatic wave, the highest possible peak-to-trough wave height is around 0.1 m, or higher for mid-range frequencies, but drops at the extremes of the range. Since the tank was devised to simulate sea states at a nominal 1:100 scale, these figures correspond to a full scale wave period range of 6–20 s, and a maximum wave height of 10 m.

For low frequencies (long waves), wave height is constrained by the maximum stroke of the wavemaking paddles. As one reduces the frequency, greater paddle displacements are required to sustain the same wave height, and eventually the paddles hit their end stops. According to first-order wavemaker theory for a 2D bottom hinged paddle, the (far-field) wave height $H_{\max}$, for regular monochromatic waves, corresponding to a maximum (water-level) stroke length of $S_{\max}$ is [30]:

$$H_{\max} = \frac{2S_{\max}}{kh_o}\left[\frac{\sinh(kh)(h_o k\sinh(kh) - \cosh(kh) + \cosh(k(h-h_o)))}{\sinh(kh)\cosh(kh) + kh}\right], \tag{1}$$

where h is the water depth, h_o is the hinge depth, and k is the wavenumber, which is related to the angular wave frequency ω by the dispersion relation:

$$\omega^2 = gk\tanh(kh). \tag{2}$$

On the other hand, for high frequencies (short waves), the wave height is constrained by wave breaking. As the frequency is increased, the wave steepness draws nearer to the breaking limit given by Miche [31] for monochromatic waves:

$$\left(\frac{H}{L}\right)_b = 0.142 \times \tanh(kh), \tag{3}$$

where H is the wave height, L is the wavelength, and the subscript 'b' indicates breaking conditions.

Re-writing Eq. (3) for the breaking wave height H_b one gets:

$$H_b = \frac{0.284\pi}{k}\tanh(kh). \tag{4}$$

An experimental programme was carried out in the curved tank to measure the achievable wave height over the design frequency range, comparing it with the theoretical limits outlined above. Measurements were made at frequencies separated by 0.1 Hz; at each

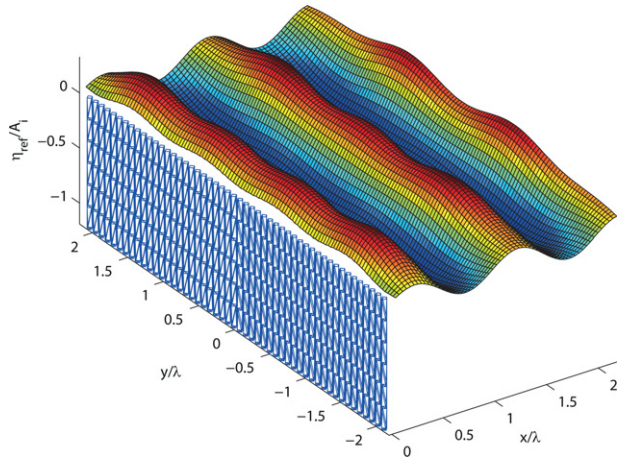

Fig. 4. Reflected waveform from model of beach for an incident wave of frequency 0.75 Hz.

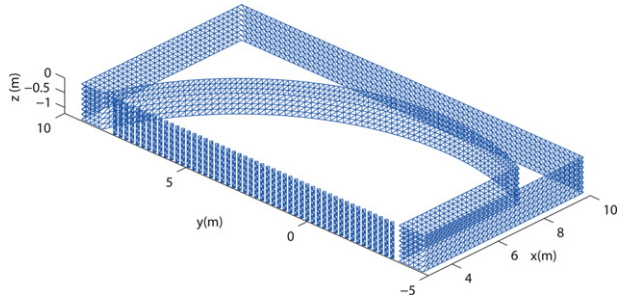

Fig. 5. Complete model of tank.

frequency of interest, the wavemaker was instructed to generate a regular wave of angle 0° (so propagating normally to the beaches). A potentiometer was attached on paddle 13, which faces the beaches, to monitor the stroke length. The paddle amplitudes were then gradually increased until a stroke of $S_{max} = 0.1$ m (within the safe operating limits of the paddles) was reached, or wave breaking occurred in the tank. Once the maximum wave height was attained in this way, wave height measurements were taken at six, fixed points in the tank, and their average computed.

Fig. 3 plots the wave height limits suggested by Eqs. (1) and (4), together with experimental measurements, versus the frequency range of the tank. The region of the graph where waves can be considered to be linear, given the wave steepness ($H/L < 0.04$), is also indicated [32].

At low frequencies, one can see a reasonably good agreement between 1st order wavemaker theory and the measured maximum wave height, despite the theory assuming a 2D, single-paddle scenario. As the frequency is increased, so is the attainable wave height, until a maximum of 0.12 m is reached at around 1–1.1 Hz. Here waves can no longer be considered to be linear (higher-order Stokes theory is more appropriate), yet 1st order wavemaker theory still provides reasonably good wave height predictions. The average (absolute) percentage error in the prediction over the 0.5–1.1 Hz range is 7%, with a maximum of 15%.

Beyond 1.1 Hz, as frequency (and hence wave steepness) is further increased, there is a departure from 1st order theory, and the wave height cannot be sustained. Eventually waves start breaking, with the phenomenon becoming pronounced at 1.5 and 1.6 Hz. The breaking wave heights at these frequencies are predicted well by theory.

2.2. Errors in 3D wave generation

Ideally one would like to be able to generate waves that are spatially homogenous, travelling in the prescribed directions, and are made up of the desired frequency components. However, in any wave tank, it is inevitable that the physical boundaries (including the wavemaker) will produce some undesirable effects that deteriorate the overall wave field. These effects may be categorised as follows.

2.2.1. Segmentation (finite spatial resolution) of wavemaker

Generation of perfect, regular, oblique waves would require the array of paddle faces to move as a continuous surface (and adapt a sinusoidal shape at any given time, in the case of a linear array), which is not feasible in practice. Instead, the wave making surface is composed of individual segments of finite width, and the resulting discontinuities in the velocity distribution can lead to the generation of spurious waves in directions other than the desired angle. The phenomenon is analysed in detail (for the case of a rectangular tank) in Sand [13], with Sand et al. [33] suggesting practical limits on wave frequency and direction so as to minimise spurious waves. Schaffer [34] extends the analysis to piece-wise linear and spline segmentation, and considers evanescent spurious modes, confined to the vicinity (within two/three water depths) of the paddles, in addition to the progressive ones.

For a linear array of paddles, a ratio of wavelength to wave board width (L/b) greater than two avoids the generation of progressive spurious modes. The curved tank, whilst featuring a different arrangement of wave boards, meets this condition throughout the operating range, and indeed spurious waves resulting from wavemaker segmentation have not been identified.

2.2.2. Wave board shape

Just as the velocity profile along the length of wavemaker should conform (as closely as possible) to the wave kinematics of the desired wave, the same should be true about the velocity profile of the wavemaker across the depth of the tank: the motion of the wave boards should match the horizontal orbital motion of water particles in the desired progressive wave.

As before, this is not achievable in practice, resulting in the generation of unwanted waves. The mismatch between the first-order velocity potential of the desired wave and the first-order potential at the boundary condition at the wavemaker leads to evanescent waves (at the fundamental frequency). Similarly, the difference between the second-order bound wave velocity potential and the corresponding boundary condition gives rise to second-order spurious waves (at harmonics of the desired frequency, and travelling slower than the main wave).

The deviation of the wavemaker from its mean position also contributes to the free second-order wave, and in the general case of multi-frequency, multi-directional wave generation, second-order effects lead to interaction terms–see Schaffer et al. [22] for the derivation of second-order wavemaking theory for multidirectional waves (under the assumption of an infinitely long wavemaker with infinitesimal segments).

There have been no studies to date looking at second-order free waves in the curved tank, but experimental results for a rectangular, shallow water tank can be found in Zaman et al. [25]. Second-order free waves are shown in the context of a numerical, rectangular wave tank in Le Touze et al. [35].

2.2.3. Finite length of wavemaker, finite domain

The finite length of a snake-type wavemaker introduces diffraction effects, leading to spatial variations in the wave height, as illustrated in Spinneken et al. [2] using a theoretical model. Reflections off the boundaries of the tank can deteriorate the wave field further.

In the curved tank, diffraction and reflections off the glass sidewall limit the angular range of waves that can be accurately generated, as quantified below. Reflections off the absorbing beaches also become significant at low levels of wave steepness – see Section 3.3 for more details.

2.3. Accuracy of wave fronts

Complex (pseudo-random) directional seas are created by combination of a number of wave fronts, each with a target height, frequency, angle and start phase associated with it. In the single summation method [36], where each frequency has only one direction, it is typical to use 32 wave fronts in a frequency band to obtain realistic enough seas [37]. Taking a directional spread of 60° in the spectrum, this equates to a spacing of less than 2° between neighbouring wave fronts. Hence, a high level of accuracy is required in the propagation angle of waves to be able to reproduce a desired sea state.

Pascal et al. [38] assessed the angular accuracy of the curved tank over the [30°; +30°] range of wave directions, and found it to achieve sub-degree accuracy in the range [−20°; +20°] (as measured with respect to the x-axis show in Fig. 2). For target wave angles greater than ±20°, the accuracy deteriorates to 2–3° because of the finite length of the arc of wavemaker segments, and effects such as reflections from the glass wall.

Complementing the work on angular accuracy, a study was carried out assessing the uniformity in wave elevation of regular and irregular waves in the curved tank [39]. Regular waves with three different wave frequencies (0.75, 1 and 1.5 Hz) and wave directions (−30°, 0°, +30°), and Pierson–Moskowitz spectra with 1 Hz peak frequency, were assessed over a 2 m × 6 m area in the tank. To quantify spatial variability, measurements of root-mean-square wave elevation η_{RMS} were taken at 48 distinct points in the domain, and the sample standard deviation of η_{RMS} was normalised by the average of η_{RMS}. The variation in wave height was measured to be 3.5% for irregular waves and between 5 and 10% for regular, 0° waves, increasing to 20–30% for ±30° waves. Good repeatability was observed in wave elevation measurements.

Due to the method of generation, all sea states have an associated repeat time, which is closely related to the separation in the individual frequency components. More precisely, the repeat frequency is given by the greatest common divisor of the frequency components. The demand signals sent to the paddles are digitally synthesised (at 32 Hz), so accurate frequency spectra, with closely spaced frequency components, may be built up in the tank, at the potential cost of a long experimental time.

3. Modelling the curved tank

3.1. The boundary element method

Numerical prediction of wave-body interactions is crucial as a design tool in the offshore industry, with the boundary element method (BEM) being the most commonly used approach. The method, based on potential flow theory, involves reformulating the equations for the potential field into a boundary integral equation via Green's theorem. Next, the integral equation is discretised and solved numerically, first to find the velocity potential on the body boundary, and then at any point in the fluid domain.

The BEM software package WAMIT is used here to model the tank. The package has been applied to wide variety of hydrodynamic problems involving floating or submerged bodies in waves; from computing the wave loadings on coastal/offshore structures [40], to the analysis of ship motion [41] and wave energy converters [42]. It has also been used, in Newman [28], to simulate wave generation and absorption in rectangular and circular wave tanks, with an array of wave-making paddles along the perimeter.

The modelling approach of Newman [28] is followed here and adapted for the geometry of the curved tank. Aside from the key assumptions of potential flow theory (incompressible, constant density, inviscid, irrotational flow), WAMIT assumes that the oscillation amplitudes of the body and the fluid are small enough so that the body surface and free surface boundary conditions may be linearised. In other words, the fluid velocity potential and hydrodynamic pressures are derived based on geometries corresponding to the rest state.

Following the approach of [28], the higher-order method of solution is used, whereby the unknown velocity potential on the boundary surface is represented by continuous B-splines. The geometry of the submerged surface of the tank is defined analytically, with separate "patches" representing each of the wavemaking paddles, the curved wall under the paddles and the glass viewing wall (WAMIT subdivides "patches" further into "panels", which may be reduced in size until a converged solution is attained). The dimensions of these elements were taken from a CAD model of the tank, and verified using on-site measurements. Water depth is taken to be constant ($h = 1.2$ m) throughout the tank.

The centre of the paddle front faces (see Fig. 2) is used as a common reference point between the model and the real tank. A Cartesian coordinate system is defined (as shown in Fig. 2) whose origin is at the centre of the arc, and whose x-axis is parallel to the glass window (and pointing towards the centre of paddle no.12). The z-axis (not shown in the figure) is directed upwards such that $z = 0$ at the (mean) water surface, and $z = -h$ at the bottom.

3.2. Wavemaking paddles

The tank's $N = 48$ wavemaker segments are bottom hinged, flap-type devices with an approximate width of 0.3 m, and hinge depth $h_d = 0.5$ m. In the WAMIT model, they are represented by vertical patches of rectangular shape that are positioned side-by-side, with no gaps in-between.

The motion of each paddle is described by a generalised mode, which specifies the normal velocity on the paddle face as a function of vertical position (with the normal velocity associated with the mode being zero elsewhere on the boundary surface of the tank). This velocity profile represents a boundary condition for the radiation potential of the wavemaking paddles and together with the free surface condition allows WAMIT to evaluate the radiation potential for each paddle [28].

The radiation potential, in turn, allows the hydrodynamic pressure (on S or in the fluid domain) and free surface elevation to be established via the linearised Bernoulli equation and the dynamic free surface condition, respectively – see Lee et al. [29] for more details. The program calculates added-mass and damping coefficients describing the hydrodynamic cross-coupling between the different modes of oscillation or, in this case, the different paddles. Furthermore, the contribution of each mode to the free surface elevation at any specified point is calculated. The free surface elevation is given as a complex quantity, as it has both an amplitude and a phase (relative to the paddle motion) associated with it.

3.3. Beaches

To allow for a uniform, progressive wave system to be established, the waves generated by one side of a wave tank must also be absorbed when they reach the other side. An important distinction between the curved tank, and the circular and rectangular tanks analysed using WAMIT in [28], is that the curved tank does not have wavemaker segments all around its perimeter. Whereas in the said paper the wavemaker is entirely responsible for both the generation and absorption of waves, in the curved tank this is not possible. Therefore, a bank of passive, wave-absorbing beaches is used, as shown in Fig. 2. Their construction is described in detail in Taylor [1].

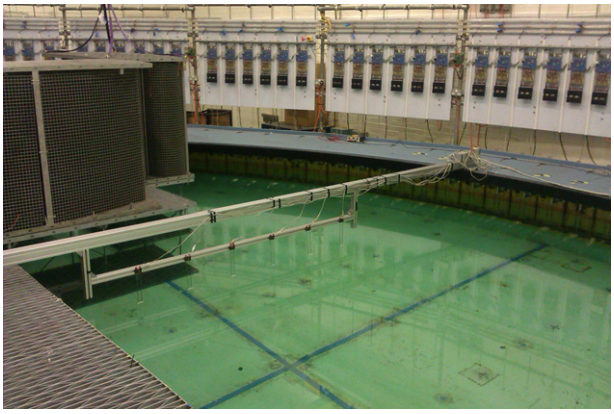

Fig. 6. Frame for wave height measurements.

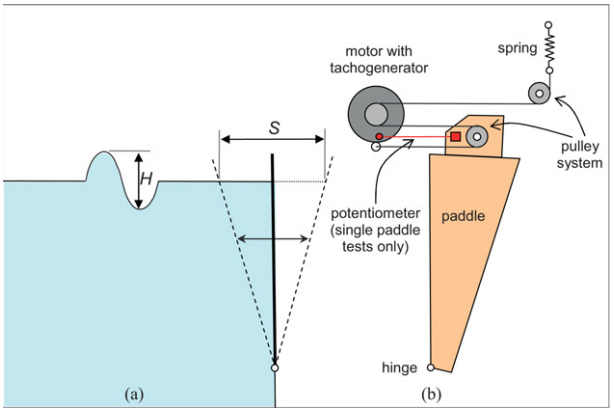

Fig. 7. (a) Definition of the paddle stroke S and (b) schematic of the wavemaker including the potentiometer and tacho-generator.

There are a number of studies in literature on the modelling of porous, wave-absorbing bodies. These range from analytic work using linear potential flow theory (e.g. Zhu et al. [43]) to computer simulations involving numerical wave tanks based on the Navier–Stokes equations [44].

Here an alternative approach is adopted that fits within the framework of WAMIT, and is consistent with experimental observations. Pascal [38] carried out a study of the beaches' reflection coefficient for normally incident, mono- and polychromatic waves. Values of $R_{\text{coeff}} > 10\%$ were recorded for low steepness ($H/L < 0.01$) waves, with values reducing markedly ($R_{\text{coeff}} < 5\%$) at higher wave steepness, and also in the polychromatic case.

In view of these findings, for most of the simulations, the beaches are modelled by an "opening" in the model of the tank (where waves leave the domain of interest, and do not return). In other words, perfect absorption is assumed. However, in cases where low frequency, low amplitude waves are generated, a partially reflecting structure is inserted into this opening.

The structure consists of an array of 50 vertical columns, positioned so that they are roughly aligned with the troughs in between the beach "wedges". Adjusting the diameter and separation of the columns allows a reflection coefficient to be obtained that matches with real-life measurements for low steepness waves. The array provides, to a fair approximation, a spatially uniform reflecting surface, as shown in Fig. 4, which depicts the reflected waveform η_{ref}, as calculated by WAMIT, when a planar wave of amplitude A_{i} and frequency 0.75 Hz is incident on the array. In this example, the normalised radius of the columns is $r/L = 0.025$, and the distance between their centres is $a/L = 0.085$ (where L is the wavelength). The resulting reflection coefficient is approximately 28%, with a lateral variation of $\pm 3\%$ in the vicinity of the structure (part of the variation being due to edge effects resulting from the finite length of the array).

The complete model of the tank is shown in Fig. 5; the additional patches around the curved section of the tank and the glass wall are to "close" the geometry, as WAMIT requires all patches to have a "wet" side and a "dry" side.

4. Validation of the BEM model

4.1. Experimental setup and procedure

To carry out meaningful comparisons between the wave field estimated by BEM, and the true wave height seen in the tank, one needs to measure the amplitudes and phases of the oscillating paddles, and feed this information into the model. More specifically, the separate wave field predictions for each paddle should be adjusted according to the measured paddle motion, before being superimposed to obtain an estimate for the overall wave field.

In the first instance, it was decided to drive one paddle at a time, and track its position, whilst measuring the resulting waves at fixed points in the tank. It was of interest how well the waves from a single "building block" in a three-dimensional wavemaker could be predicted, especially given that the spatial variations in the wave field were likely to be much greater than in the normal, multi-paddle case. Furthermore, driving individual paddles gave the opportunity to compare experimental results not just with the BEM model but also with predictions based on analytical expressions that exist for the 3D wave field of a solitary paddle.

For each single-paddle test, all other paddles were disconnected from their control boards, and clamped together to form a reflecting surface. Three paddles were chosen for the experiment: paddle numbers 1, 12, and 24 (see Fig. 2), which are believed to be a representative selection of the paddles. To capture the paddle motion, a "string" potentiometer (Celesco SP2–50) was attached to the top of the paddle, such that it measured the horizontal displacement.

This was followed by multi-paddle tests in the wave tank was used in its normal operation, with all available paddles used to generate uniform waves. Tracking the motion of paddles using potentiometers was no longer practical, so the paddle motions were instead derived from the tacho-generator outputs of the respective motors (as recorded by the wave-making system).

In both series of tests, wave height measurements were taken using a set of six resistive wave gauges connected to the WG8 system [45]. To facilitate measurements at a number of points, the wave gauges were attached to a movable frame composed of a horizontal beam with an upside-down gantry, spanning the distance between the wavemaker and the beaches. The setup can be seen in Fig. 6.

For each set of measurements, the beam was positioned parallel to the glass window, and then moved laterally through different "stations", as indicated by markings on the working platform and the beaches (the guidelines were created with the help of a laser levelling tool).

Fifteen main stations were marked out initially for the low frequency, single paddle tests, such that the measurement points formed a rectangular grid with pitch 0.4 m. Points near the glass window were more closely spaced. The array of points covers an area of 2 m $\times$ 5.4 m encompassing the region in the tank most commonly used for model testing. The measurement area was subdivided further in later tests to ensure that the wave field was adequately captured. This resulted in a total of 46 stations, and 276 separate measurement points (see Fig. 2).

The output of the position-sensing potentiometer and those of the wave gauge conditioning box were connected to the data acquisition system comprising a NI USB6259 board, sampling at 64 Hz, linked to a PC running LabVIEW.

Before each day of wave measurements, the gantry supporting

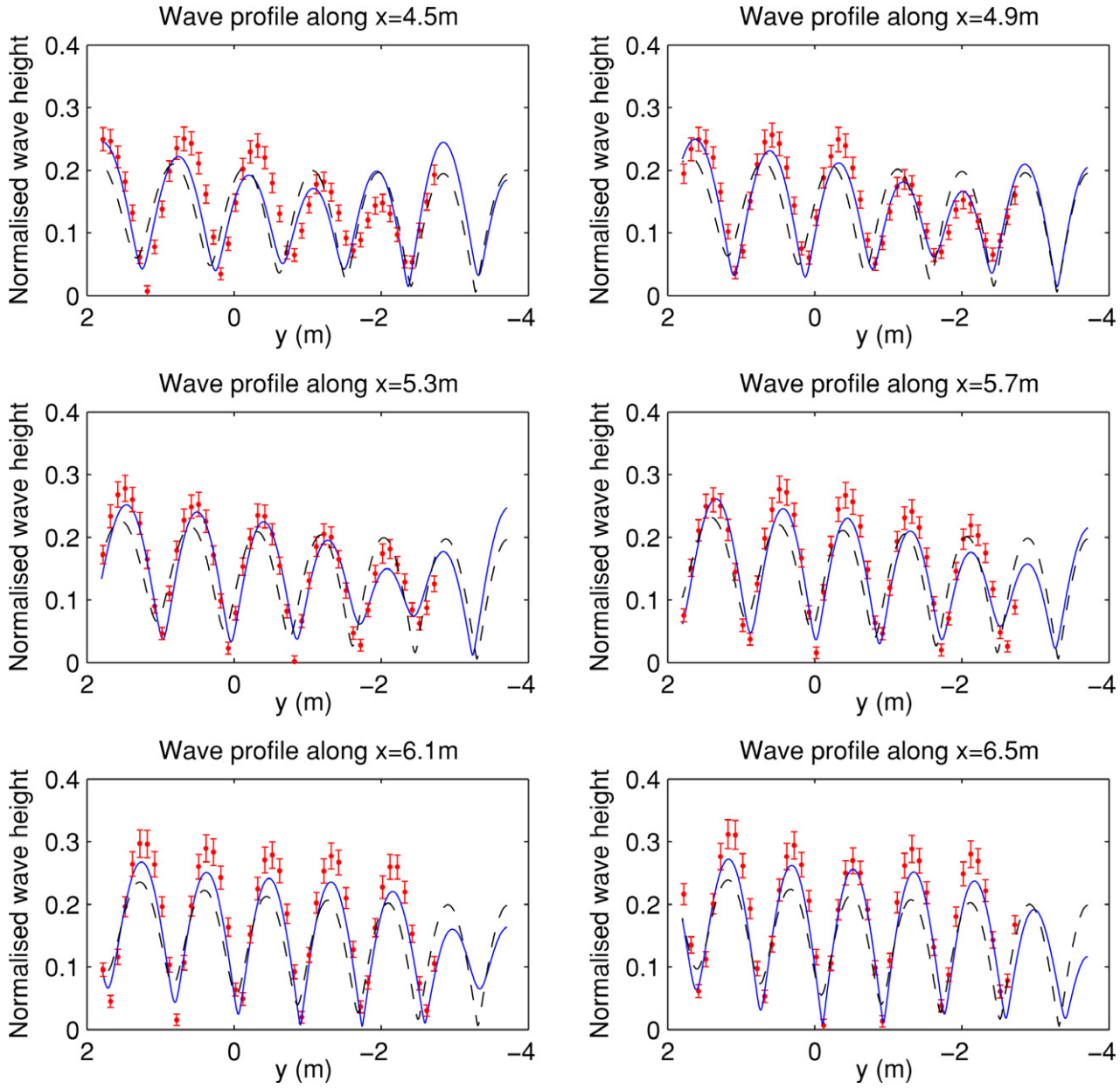

Fig. 8. Results for paddle 24 at 1 Hz: measured wave height (points with error bars) versus prediction of BEM model (full line) and simplified model (dashed line) along cross-sections of the test zone.

the wave probes was removed and attached to an automated wave gauge calibration rig (connected to the same data acquisition system described above). The rig lowers probes into the water at pre-defined steps, whilst taking accurate displacement measurements, thereby allowing the gain of the probes to be determined. The day-by-day variation in probe gain was found to be up to 2%, highlighting the need for frequent calibration.

4.1.1. Single paddle tests

With the paddle of interest (no. 1, 12 or 24) wired up with the position sensor, wave measurements were carried out in the following sequence:

- The measurement frame was laid down onto "station 1" (as indicated by the floor markings).
- Data capture from the wave gauges and the paddle position sensor was then activated, and the wavemaker software was instructed to produce a regular wave of height $H = 0.06$ m and frequency $f =$ 0.75 Hz (with only one paddle being active, the true wave heights seen in the tank would be lower than this).
- The resulting paddle motion and wave elevations were recorded for 90 s, allowing sufficient time for the wave field to become established. The paddle was then stopped, and a waiting time imposed, until the tank settled and the wave probes were measuring fluctuations of less than 0.5 mm peak-to-peak. The settling time was found to be around 1 min. Once the tank settled, the paddle was activated again, now at a frequency of 1 Hz and the measurements were repeated. Measurements were also carried out for a paddle frequency of 1.25 Hz.

The sequence was subsequently repeated for all 15 main "stations" of the measurement frame, and carried out for paddle numbers 1, 12 and 24.

In cases where the spatial variability of wave height was found to warrant more closely spaced sampling (so a greater number of

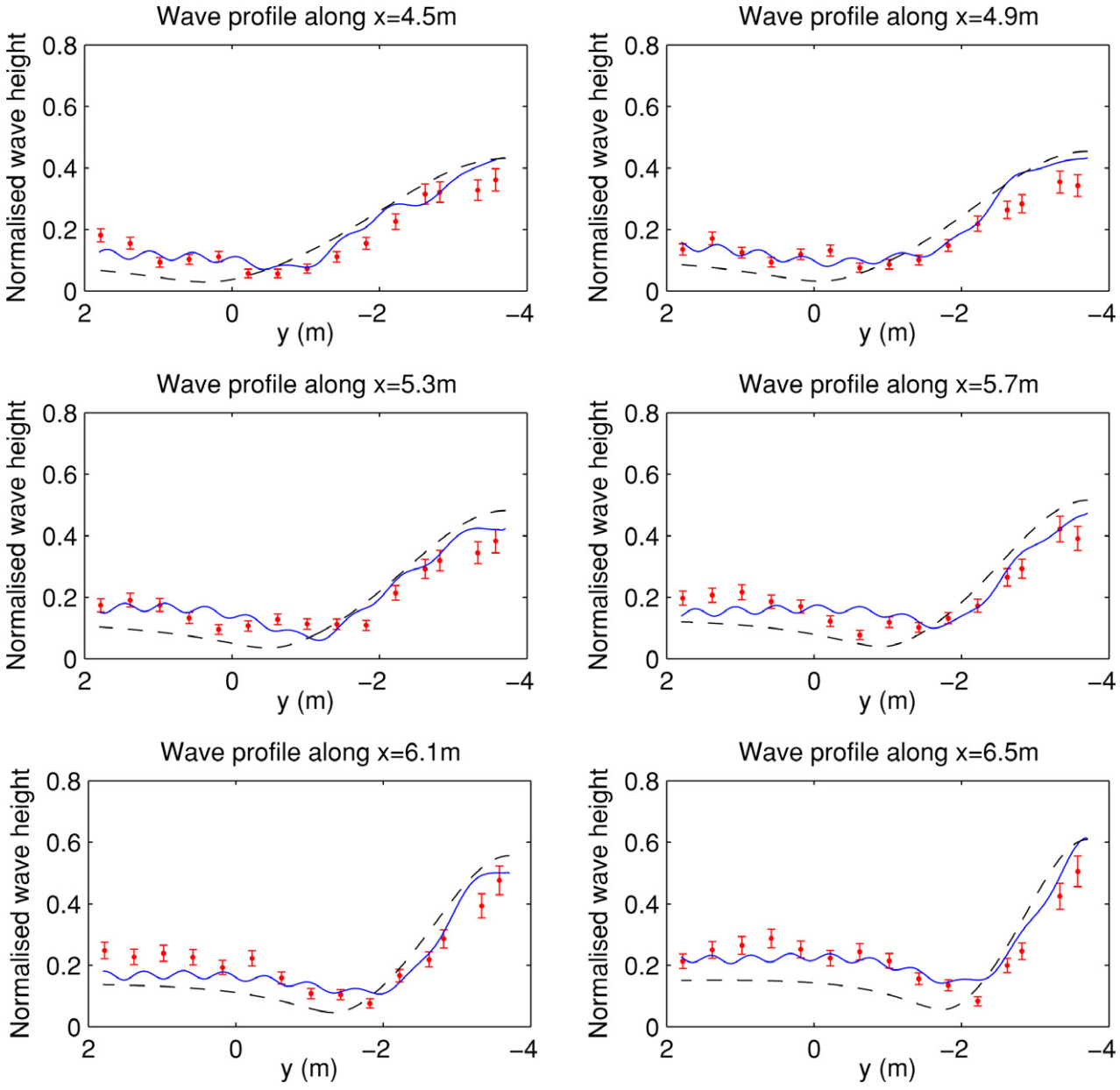

Fig. 9. Results for paddle 1 at 1.25 Hz: measured wave height (points with error bars) versus prediction of BEM model (full line) and simplified model (dashed line) along cross-sections of the test zone.

measurement frame "stations"), a different experimental procedure was adopted. The wave-making paddle was left oscillating at a certain frequency, whilst the frame was moved from one station to the next, 46 in all, stopping long enough at each station (approximately 1 min) for accurate wave height measurements to be obtained.

4.1.2. Multi-paddle tests

The tests involving multiple paddles were conducted in a similar way to the single paddle tests, with increased spatial sampling. This time, regular waves with different directions, as well as frequencies, were specified in the wavemaker software. The height demand for each wave was $H = 0.03$ m.

Table 2 specifies the main test cases in the experiments.

4.1.3. Signal processing and error analysis

The wave height at the fundamental frequency was used as the main measure of wave elevation, and was obtained by applying a Fast Fourier Transform (FFT) to the wave gauge recordings. Care was taken so that the analysed data segment always contained an integer number of cycles of the frequency of interest (the typical data length was 28 s). The standard deviation of the recorded waveform was also computed to give an additional measure for wave elevation. This metric will be referred to as the overall, root-mean-square (RMS)

Table 2
Matrix of test scenarios. Tests whose results are presented here are indicated by a black square.

	Single paddle			Multi-paddle		
	Paddle no.			Wave direction (°)		
Freq. (Hz)	1	12	24	−25	0	25
0.75	□	■	□	□	□	■
1	□	□	■	□	■	□
1.25	■	□	□	■	□	□

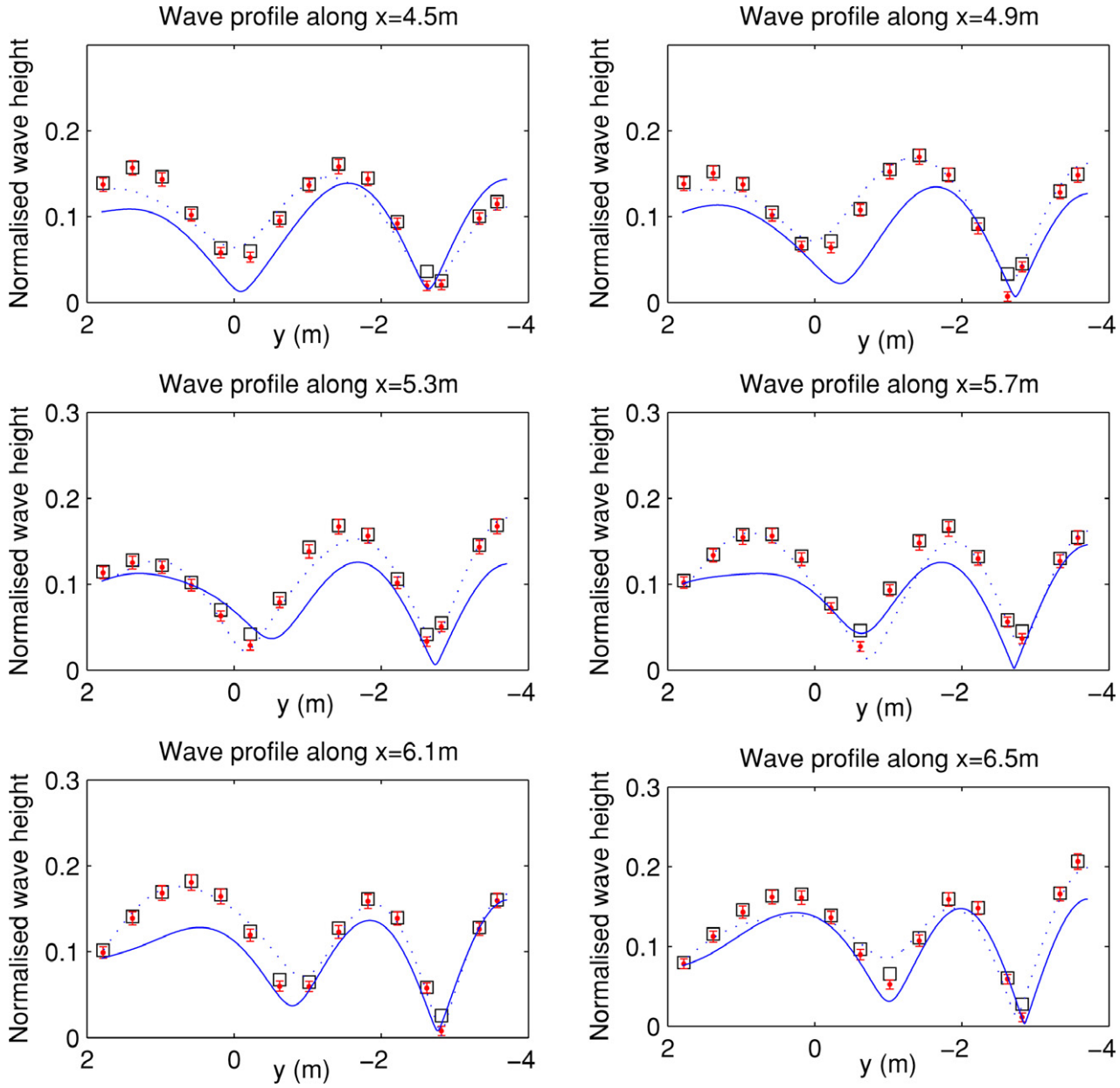

Fig. 10. Results for paddle 12 at 0.75 Hz: measured wave height of the fundamental (points with error bars) and measured RMS elevation (squares), versus prediction of basic BEM model (full line) and BEM model with beaches (dotted line) along cross-sections of the test zone.

elevation.

To get the corresponding paddle amplitudes (and phases), the FFT was also applied to the string potentiometer and tacho-generator signals. Conversion factors were worked out linking the amplitudes of said signals to the paddle stroke S at the still free surface level. Fig. 7 depicts the paddle stroke, as well as the positions of the potentiometer and the tacho-generator within the wavemaker mechanism. Strictly speaking, the tacho and potentiometer sensors capture the overall travel of the paddle, which is in an arc, rather than just the horizontal deviation, but for a typical stroke length of 0.1 m, the difference between the two is less than 0.2%.

There are a number of sources of uncertainties in the experiment, which will now be quantified. The wave gauges have a nominal accuracy of $\pm 0.1\%$ of full range, which equates to ± 0.3 mm (the data from the calibration tests would suggest even higher accuracy). For the string potentiometer, the quoted accuracy is $\pm 0.25\%$ of full stroke (approximately 1.25 m), corresponding to a ± 2.2 mm displacement at water level. The tacho-generators of the paddle motors have been individually calibrated but are nevertheless estimated to have a tolerance of $\pm 2\%$ in their voltage constants. There will also be errors in the position of the measurement points; these are estimated to be ± 5 mm at most.

Although the errors specified above are systematic, the error in the measured wave height, for instance, will vary from wave gauge to wave gauge, as well as with the wave height itself, and the same goes for paddle amplitude measurements. Similarly, every measurement point will have a different positional error associated with it.

In the single paddle tests, when evaluating the gain (or "amplitude transfer function") between the paddle stroke and the wave height at a given point in the tank, the estimate is affected by the errors in both the paddle and wave height measurements. As these errors are independent, they may be combined in quadrature to obtain a measure of the overall error in the gain estimate. Taking e_F, e_H and e_S to be the errors in the transfer F, the wave height H and paddle stroke

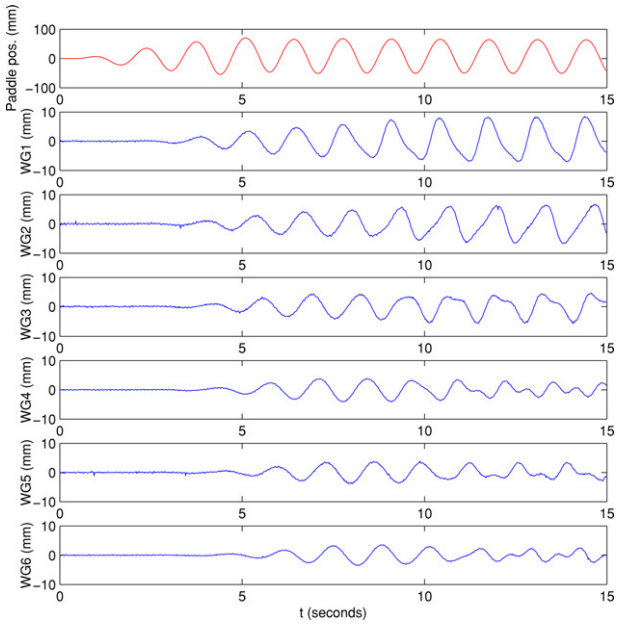

Fig. 11. Surface elevation recordings when paddle 12 is activated at 0.75 Hz.

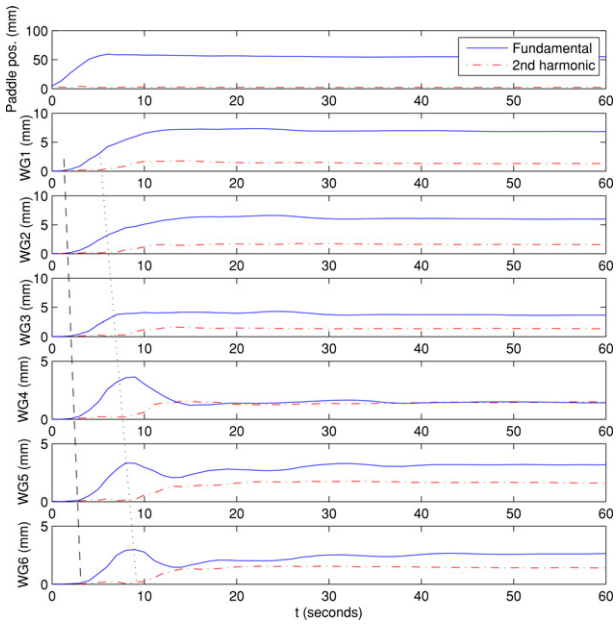

Fig. 12. Time-variation of spectral components in surface elevation recordings when paddle 12 is activated at 0.75 Hz.

S, respectively, one may write:

$$\left(\frac{e_F}{F}\right)^2 = \left(\frac{e_H}{H}\right)^2 + \left(\frac{e_S}{S}\right)^2. \tag{5}$$

When testing with multiple paddles, the wave height profile predicted by the BEM model is subject to the errors in determining the amplitudes of the individual paddles (due to the tolerance in the tachometers). An error band (or confidence interval) is therefore calculated by carrying out a series of simulations in which random deviations, representing the tachometer tolerance, are imposed on each of the paddle amplitudes.

Note that measurements (whether by the wave gauges, potentiometer or tachometer) are also subject to random, electronic noise. However, due to measurements being carried out over a number of wave periods, the resulting variance in the measured quantities was found to be negligible in comparison to the other sources of error.

4.2. Single-paddle results

Representative results are presented in Figs. 8–10, involving different paddle and frequency combinations. Each figure is composed of six subplots, with each subplot comparing the measured steady-state wave height from a row of measurement points (see Fig. 2) to the wave height profile predicted by the BEM model. Wave heights are normalised with respect to the paddle stroke, and are those of the fundamental component. Error bars have been added to the measurement points indicating the estimated error (based on the above analysis).

Included also in Figs. 8 and 9 are wave height predictions computed using a simplified linear hydrodynamic model, based around the theory presented in Takayama [14] for a single segment wavemaker in a wall (but with a hinge depth different from the water depth). To account for the reflections off the glass wall, a second "mirror image" paddle is introduced on the other side of the glass panel. Note however that any reflections off the curved arc of paddle faces are effectively ignored in this simplified model.

Fig. 8, for paddle 24 oscillating at 1 Hz, shows a good correspondence between measurements and the BEM model (full line); the measurement points follow the variations in the predicted wave profile, even if the BEM model tends to somewhat underestimate the wave heights in the tank. The simplified model (dashed line) is also surprisingly good in reproducing the measured wave height variations. However, it is less accurate than BEM overall, especially along the two lines of measurement points closest to the wavemaker (bottom plots), where BEM gives a better prediction of the height of nodes and anti-nodes.

A similar picture is presented by Fig. 9, which gives the results for paddle 1 oscillating at 1.25 Hz. The measured wave heights display similar spatial variation to that predicted by the BEM (full line) and simplified (dashed line) models. Again, BEM is more accurate than the simplified model, with the BEM predictions lying closer to the measured values virtually everywhere across the test domain.

Fig. 10 shows the results for paddle 12 moving at 0.75 Hz. At this frequency, wave steepness is rather low so the reflections off the absorbing beaches become significant. As a result, there are considerable deviations between measurements and the basic BEM model (represented by the full line). By accounting for beach reflections in the BEM model (dotted line), a much better fit can be obtained.

Aside from inaccuracies in the modelling of the beaches, another possible source of error is the effect of the gaps between paddles, whose size is around 10% of the paddle width, but which are ignored in the model. Salter [46] observed sloshing in these gaps when steep waves were generated. Moreover, whilst the clamped paddles are assumed to be completely still in the model, in reality the hydrodynamic forces acting on them induce some motion, leading to additional radiated waves. In later tests, the induced motion in the paddles beside the driven paddle was found to have an amplitude up to 10% of the driven paddle, with the amplitude reducing for paddles further away from the driven paddle.

4.2.1. Harmonic content in measurements

So far only waves at the fundamental frequency have been considered. However, in accordance with Stokes wave theory, waves at any given frequency will also have bound harmonics associated with them (travelling at the same phase velocity), the harmonics becoming more prominent for steeper waves. Moreover, as discussed in Section 2.2, in any wave tank second (and higher) harmonic *free* waves will be generated due to second-order effects at the wavemaker (un-modelled

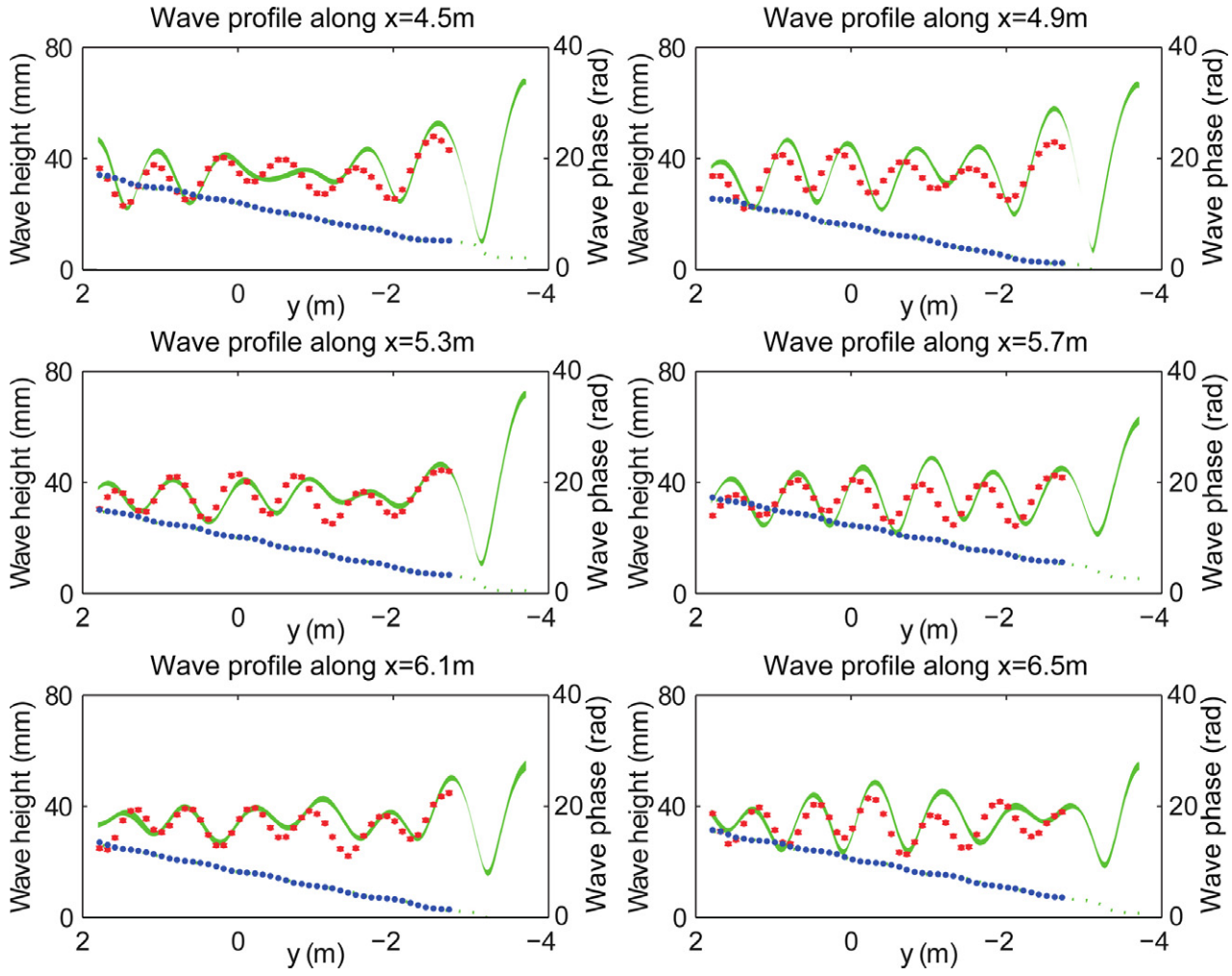

Fig. 13. Multi-paddle results for 1.25 Hz regular wave at −25°: measured wave height (red points with error bars) versus BEM model prediction (green band), and measured phase (in radians, blue points) against BEM phase (green dotted line), along cross-sections of the test zone. (For interpretation of the references to colour in this figure legend, the reader is referred to the web version of the article.)

by the first-order BEM model used here), the spurious waves propagating *more slowly* than the main wave.

The presence of spurious waves can be spotted in Fig. 10, where a measure of the overall RMS elevation (normalised by the RMS paddle displacement, and indicated by squares) has been plotted alongside the wave height measurements at the fundamental (normalised by the paddle stroke; points with error bars). One notes that at troughs (nodes) of the wave height contour, the normalised, overall elevation is noticeably greater than the normalised wave height of the fundamental.

To give a better illustration of the phenomenon, it is worth considering transient waves in the tank. Fig. 11 shows a sample of the captured wave data: the first 15 s of wave gauge recordings from the moment paddle 12 is switched on and driven at 0.75 Hz. The figure is composed of seven subplots; the uppermost plot shows the paddle position and the remaining plots depict the outputs of each of the wave gauges (which have been positioned so that they are roughly in line with the paddle, WG1 being the one closest to the wavemaker).

Note that, whilst the surface elevation waveforms initially appear to be sinusoidal, the waveforms get distorted after a few wave cycles. The distortion is due to the spurious second-order waves produced by the paddle, at the second harmonic. This becomes clearer when one considers the time-variation in the spectrum of the wave gauge signals. Fig. 12 plots the components at the fundamental (full line) and the second harmonic (dot-dashed line) for the same signals (paddle position and wave gauge outputs) as before, although over a longer timescale. The spectral components are extracted by applying Fast Fourier Transform over a 3 s moving window.

From the figure, it is apparent that as the paddle starts moving, and waves are "launched" across the tank, the first waves at the fundamental frequency are closely followed by (slower) waves at the second harmonic. Dashed and dotted lines are used to indicate the propagation speeds (group velocities) of the respective waves. Notice also the "overshoot" in the amplitude of the fundamental captured by wave gauges 4–6. This is likely to be caused by the arrival of reflections off the glass wall, resulting in destructive interference.

For the paddle frequency, and wave gauge locations in question, the harmonic content seen in the waves is considerable, especially at WG4, where, once the transients settle, the amplitude of the second harmonic essentially matches that of the fundamental (hence the significant distortion in the time-domain signal). Considering the whole set of measurement points, the average wave height of the second harmonic is 18% of the average height of the fundamental.

In practice, the harmonic content varies strongly with paddle frequency (and amplitude), so that the amount of distortion is not always as severe as in the example above, and in some cases is only visually perceivable at nodes (or regions of low amplitude) in the wave field.

4.3. *Multi-paddle results*

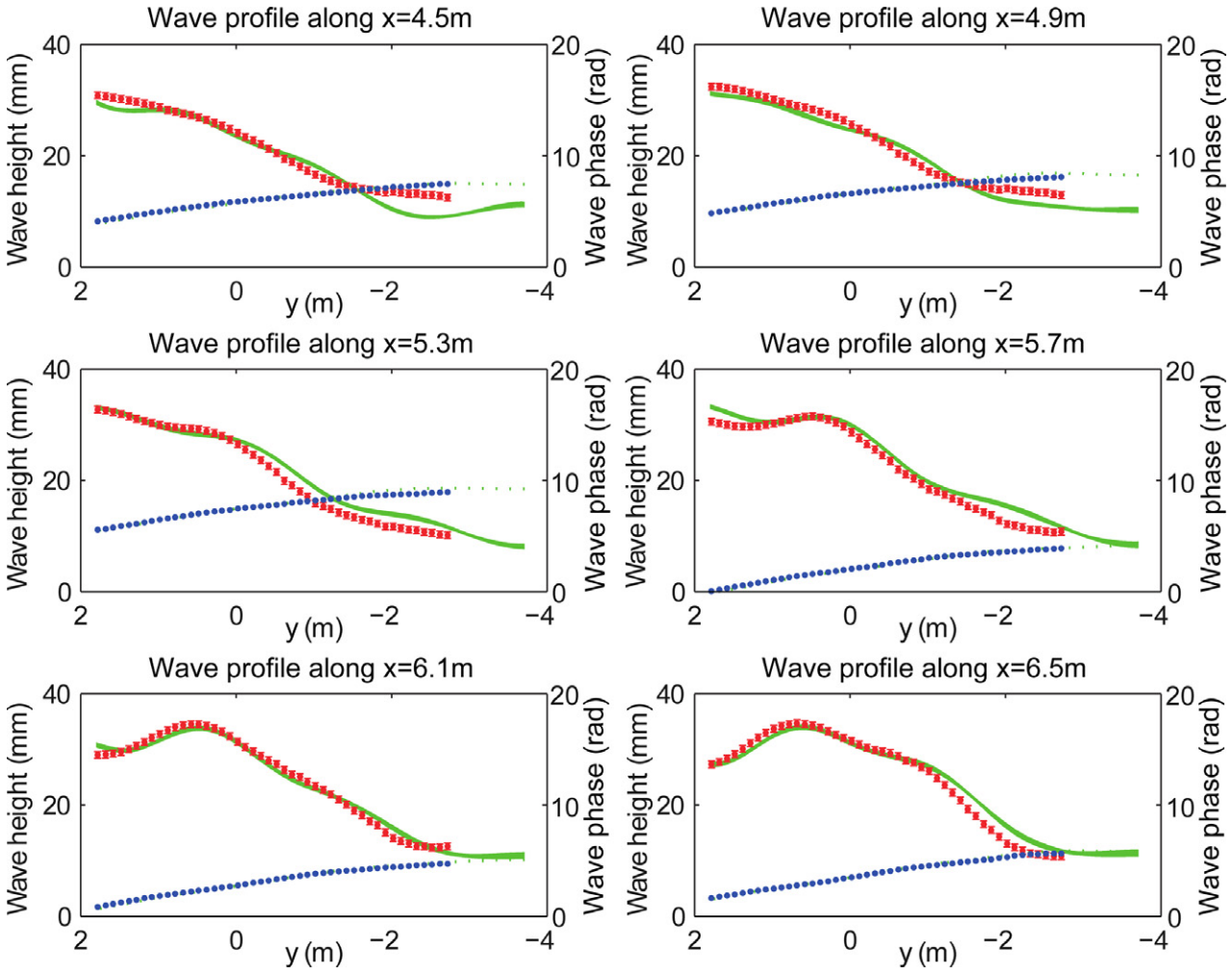

Fig. 14. Multi-paddle results for 0.75 Hz regular wave at $+25^{\circ}$: measured wave height (red points with error bars) versus BEM model prediction (green band), and measured phase (in radians, blue points) against BEM phase (green dotted line), along cross-sections of the test zone. (For interpretation of the references to colour in this figure legend, the reader is referred to the web version of the article.)

Figs. 13 and 14 show typical results for the case when regular waves are generated in the tank and compared to the prediction of the BEM model. The results are presented in a similar format to those for the single-paddle tests: the wave height data from the rows of measurement points are contrasted to wave profiles calculated using the BEM model. In addition, the wave phases – measured and predicted – are plotted. Wave heights are those of the fundamental, and the predicted height includes an "error band" that represents the uncertainty due to the likely errors in the individual paddle amplitude estimates.

The first figure is for a 1.25 Hz, -25° wave, for which the BEM model predicts ripples in the spatial wave height profile, given the observed paddle motions. The measured wave heights indeed follow the general shape of the predicted curves, although there is not a close agreement between them. In terms of the wave phase, a good agreement can be seen between the measured and predicted values, the variation of phase across the test area being consistent with the specified angle for the wave.

Fig. 14 gives the results for the case when a 0.75 Hz, $+25^{\circ}$ wave is specified in the wave-making software. As in the previous example, the general shape of the wave height contour is predicted well. The deviation between measurements and the model is most apparent in the bottom-right portion of the test zone (see Fig. 2), and could be due to un-modelled effects in the corner where the beaches and the glass wall meet. As before, the observed phase variation corresponds well to that predicted by the model.

Averaging the (absolute) percentage error in the predicted wave height over all the measurement points in the above examples one gets values of 11% and 7%.

Despite the inaccuracies in its prediction, it is argued that the model gives a fair representation of the steady-state wave field in both examples. With all paddles in action, there is significant wave content all across the tank, and a great amount of reflections (and re-reflections) off the boundary of the tank, so any inaccuracies in the dimensions of the model, or in the representation of the beaches, are likely to get magnified. Nevertheless, the model is able to predict the shape of the amplitude and phase variations across the tank.

To illustrate the challenges in modelling the absorbing beaches, a further set of multi-paddle results are presented in Fig. 15, for the case of a 1 Hz, 0° wave (so propagating normally to the beaches). Two graphs are given; the upper plot shows the wave profile, observed and predicted, along the row of measurement points closest to the absorbers. The lower graph plots the beach reflection coefficient (along with the estimated standard error), as determined from the two lines of measurement nearest to the beaches, using the method of Goda et al. [47].

The measured reflection coefficients are mostly below 5% (in accordance with the results of Pascal et al. [38]), but are seen to vary significantly across the measurement zone. Some of this variation is likely to be caused by changes in wave amplitude across the tank: the

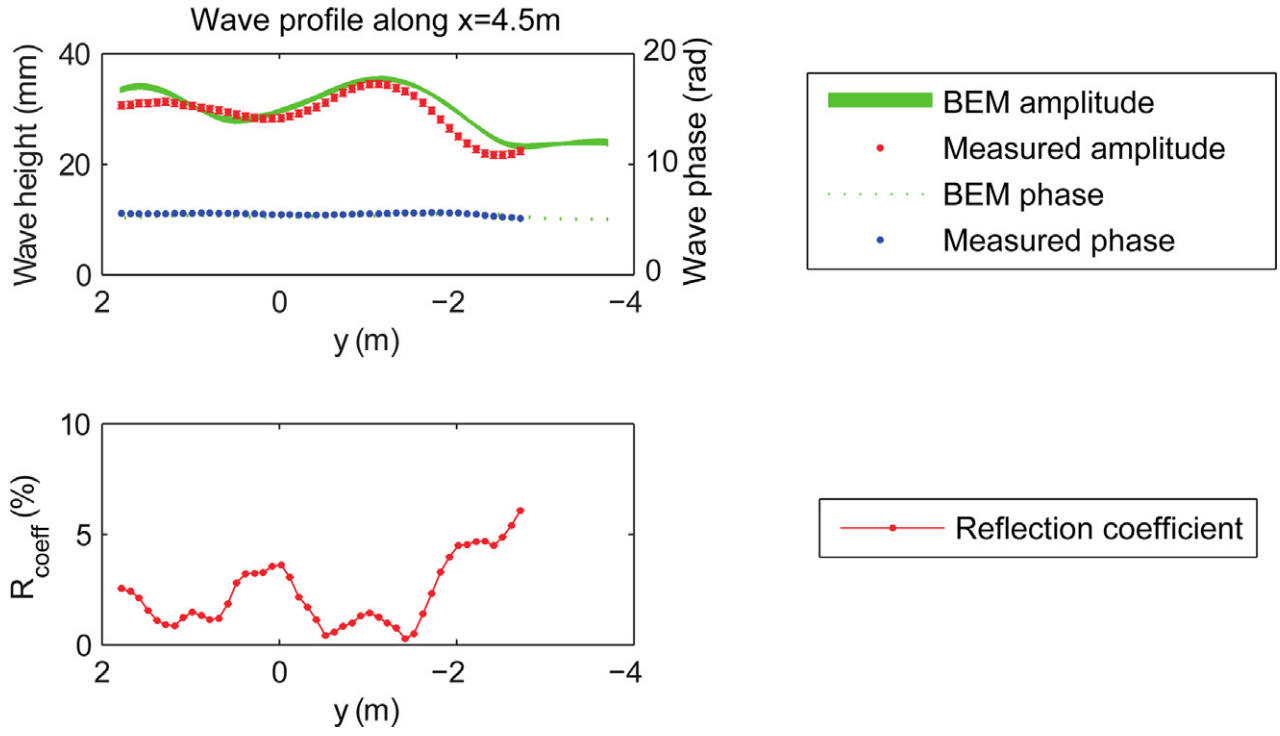

Fig. 15. Multi-paddle results for 1 Hz regular wave at 0°: upper graph compares measured versus predicted wave profile along the row of measurement points closest to the beaches, lower graph plots the beach reflection coefficient.

reflection coefficient is highest near the glass wall, where the amplitude is at its lowest. The "sawtooth" geometry of the beaches may also be partly responsible for the spatial variations in R_{coeff}.

Whilst it is possible to introduce a given reflection coefficient in the model (as discussed in Section 3.3), spatial variability (or amplitude dependence) is more difficult to model.

5. Conclusions

A boundary element method (BEM) model for the Edinburgh curved tank has been evaluated. In a series of single-paddle and multi-paddle tests, the method was found to predict the general wave profile across the tank. Whilst the wave height estimates for individual points in the domain can be inaccurate – the average absolute error is typically around 10% in the multi-paddle case – the model offers a good indication of the spatial variation in wave height and phase.

The model has two main limitations: it is based on first-order potential theory, so second-order waves are neglected, and it only provides an approximate representation of the absorbing beaches.

In the single-paddle case, a scenario not generally explored in tanks with multiple paddles, significant spurious, second-order waves are seen in the tank, especially at low paddle frequencies. For instance, when a single paddle is driven at 0.75 Hz and a paddle stroke of 0.1 m, the wave height of the second harmonic, averaged over the test zone, approaches 20% of the height of the fundamental. These second harmonic waves are un-modelled by the BEM model here.

As regards the beaches, whilst the model is able to replicate the typical reflection coefficients seen with low steepness waves, it does not reproduce the spatial variability in the coefficient, nor the likely directionality of the beaches.

The method provides a simple way for exploring the characteristics of the tank, as far as linear wave generation is concerned. It could also prove to be a useful tool in the design of future tanks, for instance in assessing the effect of different geometries and paddle widths on the wave uniformity that can be obtained in a desired "model testing zone" within the tank.

Whilst this paper focuses on the prediction of wave elevation, BEM modelling also allows the hydrodynamic loading on the individual paddles to be estimated and such could help in the design of control systems for arrays of wave boards. In current systems, it is common to use independent, identically programmed control units for each wave-making paddle, each control unit receiving an individual (amplitude or force) demand signal from a central computer. By designing a more intelligent system, that is aware of the hydrodynamic coupling between the paddles, better wave control might be achieved. Indeed, current research is concerned with turning the BEM model for the curved tank into a time-domain model, incorporating the paddle dynamics, thereby allowing transient (not just steady state) waves to be simulated and different paddle control schemes to be assessed.

References

[1] Taylor J, Rea M, Rogers D. The Edinburgh curved tank. In: Fifth European wave energy conference, Cork, Ireland. 2000, pp. 307–14.
[2] Spinneken J, Swan C. The operation of a 3D wave basin in force control. Ocean Engineering 2012;55:88–100.
[3] Maeda K, Hosotani N, Tamura K, Ando H. Wave making properties of circular basin. International symposium on underwater technology: IEEE 2004:349–54.
[4] Naito S, Minoura M, Okayama E. Diffraction force in compact basin with absorbing wave maker. International offshore and polar engineering conference 2002:399–405.
[5] Davey T, Bryden I, Ingram D, Robinson A, Sinfield J, Wallace A. The all-waters test facility – a new resource for the marine energy sector. In: 4th international conference on ocean energy, Dublin, Ireland. 2012.
[6] Naito S. Wave generation and absorption in wave basins: theory and application. International Journal of Offshore and Polar Engineering 2006;16:81–9.
[7] Jeffrey DC, Keller GJ, Mollison D, Richmond DJE, Salter SH, Taylor JRM. Edinburgh wave power project: 4th year report. University of Edinburgh; 1978.
[8] Linfoot BT, Bryden IG, Hall MS. Computer-controlled simulation of short-crested seas. ICE Proceedings 1990;89:207–24.
[9] Salter S. Absorbing wave-makers and wide tanks. Proc. symp. directional wave spectra applications: ASCE 1981:185–202.
[10] Ochi MK. Ocean waves: the stochastic approach. Cambridge, UK: Cambridge University Press; 2005.
[11] Rogers D, King GB. Wave generation using ocean and wave. Edinburgh, UK: Edinburgh Designs Ltd.; 1997.
[12] Pascal R, Bryden I. Directional spectrum methods for deterministic waves. Ocean Engineering 2011;38:1382–96.

[13] Sand SE. Three-dimensional deterministic structure of ocean waves. Lyngby, Denmark: Institute of Hydrodynamics and Hydraulic Engineering, Technical University of Denmark; 1979.
[14] Takayama T. Theoretical properties of oblique waves generated by serpent-type wavemakers. Report of Port and Harbour Research Institute 1982;21:3–48.
[15] Dalrymple R, Greenberg M. Directional wave makersPhysical modelling in coastal engineering.. Rotterdam, The Netherlands: AA Balkema; 1985, pp. 67–81.
[16] Dalrymple RA. Directional wavemaker theory with sidewall reflection. Journal of Hydraulic Research 1989;27:23–34.
[17] Isaacson M, Qu SQ. Predicted Wave Field in a Laboratory Wave Basin. Canadian Journal of Civil Engineering 1990;17:1005–14.
[18] Hiraishi T, Mansard E. Validation of a numerical diffraction model for multidirectional wave generation. Part 2. Experimental verification of the model results. In: Proceedings of the 2nd International offshore and polar engineering conference, San Francisco, USA. 1992.
[19] Isaacson M. Wave field in a laboratory wave basin with partially reflecting boundaries. International Journal of Offshore and Polar Engineering 1995;5:1–9.
[20] Suh K, Dalrymple R. Directional wavemaker theory: a special approach. In: Proc. IAHR seminar on wave analysis and generation in laboratory basins, 22nd IAHR congress, Lausanne, Switzerland. 1987, pp. 389–95.
[21] Li W, Williams AN. Second-order waves in a three-dimensional wave basin with perfectly reflecting sidewalls. Journal of Fluids and Structures 2000;14:575–92.
[22] Schaffer HA, Steenberg CM. Second-order wavemaker theory for multidirectional waves. Ocean Engineering 2003;30:1203–31.
[23] Ducrozet G, Bonnefoy F, Le Touze D, Ferrant P. A modified high-order spectral method for wavemaker modeling in a numerical wave tank. European Journal of Mechanics - B/Fluids 2012;34:19–34.
[24] Park J, Uno Y, Sato T, Miyata H, Chun H. Numerical reproduction of fully nonlinear multi-directional waves by a viscous 3D numerical wave tank. Ocean Engineering 2004;31:1549–65.
[25] Zaman MH, Peng H, Baddour E, McKay S. Spurious waves during generation of multi-chromatic waves in the wave tank in shallow water. In: Proceedings of the ASME 30th international conference on ocean, offshore and arctic engineering, vol. 6. 2011, pp. 909–17.
[26] Minoura M, Naito S, Muto T, Okuyama E. Generation of arbitrary wave field in arbitrarily configured wave basin composed of element-absorbing wavemakers. International Offshore and Polar Engineering 2011;21:272–9.
[27] O'Dea JF, Newman JN. Numerical studies of directional wavemaker performance. In: 28th American towing tank conference, Ann Arbor, MI, USA. 2007.
[28] Newman JN. Analysis of wave generators and absorbers in basins. Applied Ocean Research 2010;32:71–82.
[29] Lee C, Newman J. WAMIT® user manual, version 7.0 PC. Chestnut Hill, MA, US: WAMIT, Inc.; 2012.
[30] Frigaard P, Hgedal M, Christensen M. Wave generation theory. Aalborg, Denmark: Hydraulic & Coastal Engineering Laboratory, Department of Civil Engineering, Aalborg University; 1993.
[31] Miche A. Mouvements ondulatoires de la mer en profondeur croissante ou décroissante. Première partie. Mouvements ondulatoires périodiques et cylindriques en profondeur constante. Annales des Ponts et Chaussées 1944;Tome 114:42–78.
[32] Hattori M. Experimental study on the validity range of various wave theories. Coastal engineering proceedings 1986;1:232–46.
[33] Sand SE, Mynett A. Directional wave generation and analysis. In: Proc. IAHR seminar on wave analysis and generation in laboratory basins, 22nd IAHR congress, Lausanne, Switzerland. 1987, pp. 209–35.
[34] Schaffer HA. Some design aspects of an absorbing 3D wavemaker. Coastal Engineering 1998;1:1082–95.
[35] Le Touze D, Bonnefoy F, Ferrant P. Second-order spectral simulation of directional wave generation and propagation in a 3D tank. International offshore and polar engineering conference 2002:173–9.
[36] Mansard E, Miles M. Experimental validation of directional wave maker theory with side wall reflections. International Journal of Offshore and Polar Engineering 1994;4:686–90.
[37] Jefferys E. Directional seas should be ergodic. Applied Ocean Research 1987;9:186–91.
[38] Pascal R, Lucas J, Ingram D, Bryden I. Assessing and improving the Edinburgh curved wave tank. In: Proceedings of the 19th international offshore and polar engineering conference, Osaka, Japan. 2009.
[39] Cruz J, Pascal R, Taylor J. Characterisation of the wave profile in the Edinburgh curved tank. In: Proceedings of the 25th international conference on offshore mechanics and arctic engineering, vol. 2. 2006, pp. 1–10.
[40] Clauss GF, Birk L. Hydrodynamic shape optimization of large offshore structures. Applied Ocean Research 1996;18:157–71.
[41] Lee S, Kim M, Lee D, Kim J, Kim Y. The effects of LNG-tank sloshing on the global motions of LNG carriers. Ocean Engineering 2007;34:10–20.
[42] Payne GS, Taylor JRM, Bruce T, Parkin P. Assessment of boundary-element method for modelling a free-floating sloped wave energy device. Part 1. Numerical modelling. Ocean Engineering 2008;35:333–41.
[43] Zhu ST, Chwang AT. Analytical study of porous wave absorber. Journal of Engineering Mechanics-ASCE 2001;127:326–32.
[44] Zhan JM, Dong Z, Jiang W, Li YS. Numerical simulation of wave transformation and runup incorporating porous media wave absorber and turbulence models. Ocean Engineering 2010;37:1261–72.
[45] Edinburgh Designs Ltd. Manual for the WG8 wavegauge conditioning box. Edinburgh, UK; 1997.
[46] Salter SH. Relocation of a multidirectional mixed wave spectrum test-tank with modifications for reduced area and minimum cross-wave errors. IGR report to EPSRC. University of Edinburgh; 2003.
[47] Goda Y, Suzuki T. Estimation of incident and reflected waves in random wave experiments. Coastal engineering proceedings 1976;1:828–45.